A&A 412, 185–198 (2003)
DOI: 10.1051/0004-6361:20031372

Astronomy & Astrophysics

Dusty ring nebulae around new candidate Luminous Blue Variables

J. S. Clark[1], M. P. Egan[2], P. A. Crowther[1,7], D. R. Mizuno[3], V. M. Larionov[4,5], and A. Arkharov[6]

[1] Department of Physics and Astronomy, University College London, Gower Street, London, WC1E 6BT, UK
[2] US Air Force Research Laboratory: MDA/AS, 7100 Defence Pentagon, Washington, DC 20301-7100, USA
[3] Institute for Scientific Research, Boston College, 140 Commonwealth Avenue, Chestnut Hill, MA 02467-2862, USA
[4] Astronomical Institute of St. Petersburg University, St. Petersburg, Petrodvorets, Universitetsky pr. 28, 198504 St. Petersburg, Russia
[5] Isaac Newton Institute of Chile, St. Petersburg Branch, Russia
[6] Central Astronomical Observatory, 196140 St. Petersburg, Russia
[7] Department of Physics and Astronomy, University of Sheffield, Hounsfield Road, Sheffield, S3 7RH, UK

Received 2 June 2003 / Accepted 2 September 2003

Abstract. We report on the discovery of a further two ring nebulae in the Midcourse Space Experiment (MSX) Galactic Plane Survey; G24.73+0.69 and G26.47+0.02. Morphologically, both appear similar to the nebulae found around the Luminous Blue Variable (LBV) candidates G79.29+0.46 and Wra 17-96. A central, unresolved point source was identified in both cases – positional coincidence with the star StRS 237 was found for G26.47+0.02, while no optical counterpart could be identified for G24.73+0.69. However, subsequent near IR broadband imaging of the G24.73+0.69 field identified a very red – $(J-K) \sim 2$ mag – stellar counterpart to the central object. Near-IR spectroscopy of both objects reveal rich emission line spectra dominated by H I, He I and low excitation metals, suggesting classification as luminous B supergiants and revealing a striking superficial similarity to the other MSX ring sources and known LBVs. We utilised a NLTE model atomsphere code to model the K band spectra and near-IR spectral energy distributions of the central stars in order to determine their physical parameters. Adopting a distance, $d = 5.2$ kpc to G24.73+0.69 yields a temperature, $T = 12$ kK, luminosity, $\log(L/L_{\odot}) = 5.6$ and mass loss rate, $\dot{M} = 1 \times 10^{-5}\ M_{\odot}\ \mathrm{yr}^{-1}$. G26.47+0.02 appears to be a more extreme object; adopting $d = 6.5$ kpc results in $T = 17$ kK, $\log(L/L_{\odot}) = 6.0$ and $\dot{M} = 9 \times 10^{-5}\ M_{\odot}\ \mathrm{yr}^{-1}$, placing it at the Humphreys-Davidson limit for massive stellar objects. Analysis of the spatially resolved mid-IR fluxes of both objects reveal extended periods of enhanced mass loss, resulting in comparatively low mass nebulae, with chemistries dominated by O-rich dust (with a population of small Fe grains existing co-spatially with the silicate dust). Comparison to the other MSX ring nebulae sources reveals a homogeneous group of objects, with both stellar and nebular properties consistent with known LBVs. With both spectroscopic and/or photometric variability observed for those sources with multiepoch observations, we propose a close affinity between both classes of object and suggest that long term monitoring of the MSX sources will reveal them to be bona fide LBVs.

Key words. stars: emission line, Be – stars: circumstellar matter – stars: winds, outflows

1. Introduction

As massive, luminous stars evolve from the Main Sequence to become hydrogen depleted Wolf Rayet (WR) stars they shed their outer H-rich atmosphere over a very short period of time. The period of enhanced mass loss is associated with the Luminous Blue Variable (LBV) phase, which is characterised by significant photometric and spectroscopic variability on timescales from months to years (e.g. Humphreys & Davidson 1994). Such variability appears to be associated with changes in the temperature and radius of the star and which in some cases – the so called "giant eruptions" – leads to increases in both the bolometric luminosity and mass loss rate of the star. The high mass loss rate associated with the LBV phase typically results in the formation of an ejecta nebula around the star (e.g. Nota et al. 1995). Six of the seven LBVs within our galaxy are identified with nebulae, while a number of other stars have been proposed as candidate LBVs (cLBV) due to the presence of chemically enriched ejecta. Such nebulae have both gaseous and dusty components, with typical expansion velocities of ~30–100 km s^{-1}. Masses of the nebulae are somewhat uncertain given the difficulty in accounting for a possible neutral gaseous component, but are typically thought to be of the order of a few $M_{\odot}$ (e.g. Figer et al. 1999 and Refs. therein).

Given the rarity of LBVs, other examples within our galaxy are likely to be found at large distances, and hence are expected to be very heavily reddened, making optical identification difficult, if not impossible. One possible technique to identify further candidates is to search for emission from circumstellar ejecta at wavelengths which are less affected by

Send offprint requests to: J. S. Clark,
e-mail: jsc@star.ucl.ac.uk

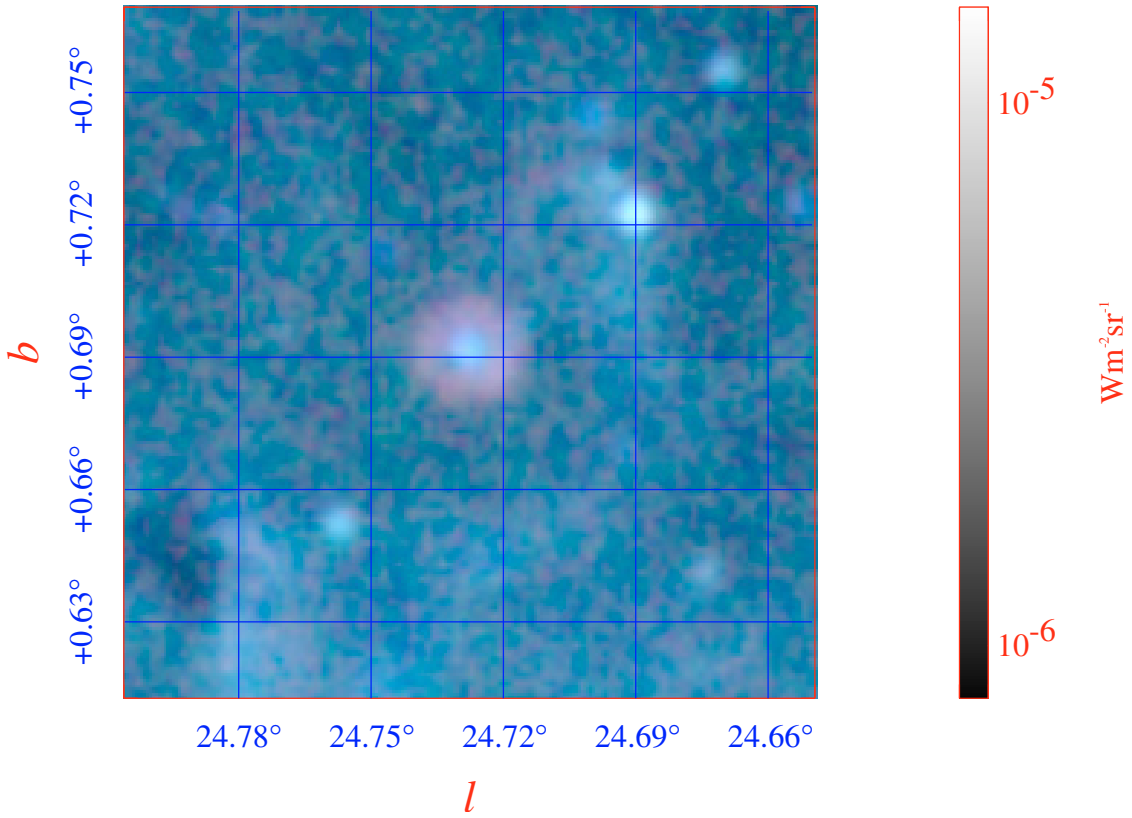

Fig. 1. Three colour image of G24.73+0.69 from MSX. *Blue*: Band *A* (6.8–10.8 μm); *green*: bands *C* and *D* (11.1–15.9 μm); *red*: Band *E* (18.2–25.1 μm). The field of view of the figure is $0.15^\circ \times 0.15^\circ$.

extinction from the ISM, such as the mid-IR (thermal emission from dust) and radio (free–free/free–bound from ionised ejecta). For example the cLBVs G79.49+0.26 (Higgs et al. 1994) and G25.5+0.2 (Subrahmanyan et al. 1994) have both been identified from radio observations while more recently the B supergiant Wra 17-96 was found to be surrounded by a massive dusty nebula (Egan et al. 2002).

Here we present the discovery of a further two ring nebulae in the MSX galactic plane survey; G24.73+0.69 and G26.47+0.02 (Sect. 2). Near-IR photometry and spectroscopy of the central, stellar sources obtained during 2001–02 are presented (Sects. 3 and 5) and the archival radio data for both sources surveyed (Sect. 4). In Sects. 6.1 and 6.2 we present quantitative analyses of both central objects and nebulae. Finally the the nature of both objects is discussed in light of prior observations of (c)LBVs (Sect. 6.4).

2. MSX observations

Mill et al. (1994) give an overview of the Midcourse Space Experiment (MSX) mission and instruments on the spacecraft. A detailed account of the characteristics of the infrared telescope and the Galactic Plane Survey on MSX can be found in Price et al. (2001). The IR instrument used five line-scanned focal plane arrays spanning wavelengths from 4.2 to 25 μm. The Galactic plane survey observations from four of the arrays are presented here: Band *A* (6.8–10.8 μm, λ_0 = 8.28 μm), Band *C* (11.1–13.2 μm, λ_0 = 12.13 μm), Band *D* (13.5–15.9 μm, λ_0 = 14.65 μm) and Band *E* (18.2–25.1 μm, λ_0 = 21.34 μm).

Table 1. Flux densities for the 2 central sources from the version 2 of the MSX Point Source Catalogue.

Source	Band *A*	Band *C*	Band *D*	Band *E*
G26.47+0.02	2.27 Jy	3.56 Jy	1.83 Jy	1.55 Jy
G24.73+0.69	1.96 Jy	1.37 Jy	1.01 Jy	0.41 Jy

MSX Galactic Plane Survey image plates (publicly available through NASA/IPAC at `http://irsa.ipac.caltech.edu`) were created by convolving the full data set of survey scans with a 7.06″ FWHM Gaussian onto the image grid, which has 6″ centers. Given the oversampling of the survey data, this pixel spacing is the smallest that can be support (within the Nyquist criterion), given the measured point response function and the system modulation transfer function. The image products have a resolution of ∼20″ taking into account inherent instrument resolution and the slight smoothing introduced by the image construction kernel. The Noise Equivalent Radiance of the different bands in the image are: ∼2 MJy/sr in Band *A*, ∼15 MJy/sr in Band *C* and *D*, and ∼35 MJy/sr in Band *E*.

In Fig. 1 we present a false colour image of the MSX in-band radiance (W m^{-2} sr^{-1}) of the approximately $0.15^\circ \times 0.15^\circ$ region containing G24.73+0.69. The 8.3 μm band is encoded in blue, the sum of the 12.1 and 14.7 μm radiance is encoded as green, and the 21.3 μm band is red. Figures 2 and 3 show the data (image and contours) at 8.3 μm and 21.3 μm, respectively, which are the two bands with the highest signal-to-noise ratio.

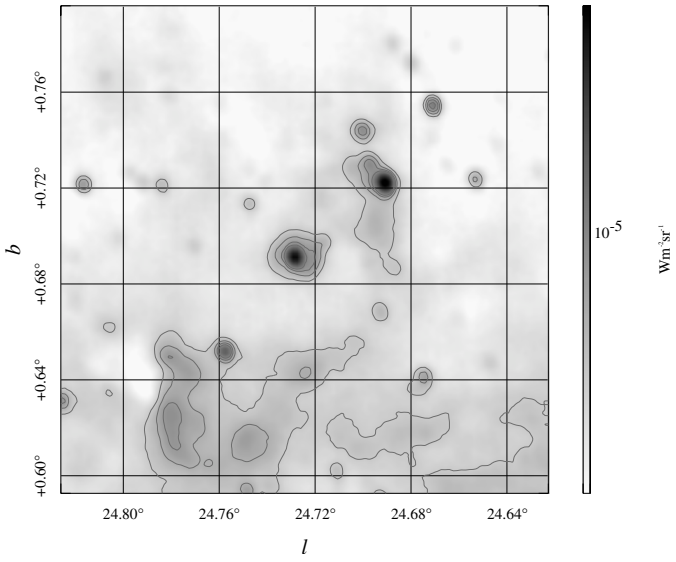

Fig. 2. Image and contours of MSX band A (8.3 μm) data for G24.73+0.69. Contour levels are 0.55, 0.7, 0.85 and 1.5 $\times$ 10^{-5} Wm^{-2} sr^{-1} and the image stretch is logarithmic between 3.5 $\times$ 10^{-6} and 2.55 $\times$ 10^{-5}.

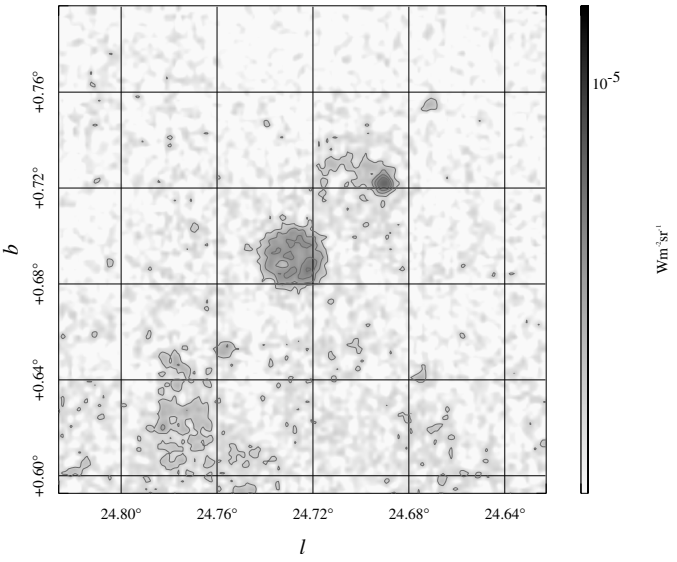

Fig. 3. Image and contours of MSX band E (21.34 μm) data for G24.73+0.69. Contour levels are 2, 3, 4 and 5 $\times$ 10^{-6} Wm^{-2} sr^{-1} and the image stretch is logarithmic between 1.2 $\times$ 10^{-6} and 1.5 $\times$ 10^{-5}.

Figures 4–6 are the corresponding figures for the 0.3° $\times$ 0.3° field containing G26.47+0.02.

The extended emission associated with G24.73+0.69 appears to be approximately circularly symmetric in all bands, with a maximal radial extent of ∼60″. Of particular interest is the presence of a second, possibly bipolar, fragmetary shell also centred on G24.73+0.69, which is most clearly visible in the Band A image and orientated ∼45° west of Galactic north. For the southerly "lobe" we find a linear size of ∼5′ $\times$ ∼2.5′. At a distance of ∼5 kpc (Sect. 6.1) these correspond to semi-major and -minor axis of ∼(7.25 $\times$ 3.6)cos(θ) pc (where θ is the angle between the major axis and the plane of the sky). In contrast to G24.73+0.69, G26.47+0.02 has a greater radial extent ($R_{\rm out}$ ∼ 80″) and is clearly bipolar, with the strongest emission in the Band E image (Fig. 6) oriented ∼30° east of Galactic north. Similar bipolarity has also been observed in a number of (c)LBV, notably in the mid-IR images of the nebulae surrounding AG Car, Wra 751 (Voors et al. 2000a) and AFGL 2298 (Ueta et al. 2001).

The central, stellar source is detected in both objects at a number of wavelengths, with fluxes given in Table 1, while in Fig. 7 we present the shell colour temperatures for both objects as a function of radial angular distance. Of interest is the apparent structure evident for G24.73+0.69, and the rather cool temperature derived for G26.47+0.02, for which the flux of the central point source peaks at 12 μm. Given that the spatial resolution of MSX is only ∼20″ it is likely that we are sampling contributions from both cool (∼10^2 K) and hot (∼10^3 K) dust (possibly in more than one nested shell) as well as a possible contribution from free–free/bound–free emission from the stellar wind of the central object (Sect. 6). Therefore, some caution should be exercised over the interpretation of Fig. 7 as it is probable that the colour temperature at a given radius does not have a simple *physical* correspondance to a unique nebular dust temperature.

3. Photometric observations

A comparison of the co-ordinates of the central objects of the MSX nebulae was made with SIMBAD and the Digital Sky Survey. A positional coincidence with the highly reddened star StRS 237 was found for G26.47+0.02 (Stephenson 1992)[1]. No optical counterpart was found for the central source of G24.73+0.69.

Given the large reddening implied for StRS 237, a series of broadband JHK images were taken of the fields of both nebulae between 2001–2002. These data were obtained at the AZT-24 1.1 m telescope in Campo Imperatore (Italy) with the SWIRCAM 256 $\times$ 256 HgCdTe detector, yelding a scale of 1.04 arcsec/pix, resulting in a ∼4′ $\times$ 4′ field of view. Examination of the field of G24.73+0.69 revealed a bright, very red point source at RA 18 33 55.5 Dec −6 58 40 (J2000) – a displacement of ∼2.8 arcsec from the central source in the MSX images. We present a finding chart for this object, which we propose to be the near-IR counterpart of the MSX mid-IR point source, in Fig. 8.

In Table 2 we present the results of the monitoring of both sources in 2001–2002. G24.73+0.69 shows clear indications of systematic variability in all wavebands at >5σ; we plot these data in Fig. 9. G26.47+0.02 (we chose to continue using this designation for consistency) shows no variability at the 5σ level in the J and H bands, and is only marginally variable at this level in the K band over the course of the observations. However, comparison to the 2 mass data suggests that G26.47+0.02 *was* variable at the ∼0.3–0.5 mag. level between the epoch of 2 mass observations (1997–2001) and our data (2001–2002).

[1] An R band finding chart for StRS 237 is presented by Stephenson (1992); note however that the finding chart is in error, with the star corresponding to the co-ordinates given by Stephenson (1992) being the the bright object directly *east* of the star indicated.

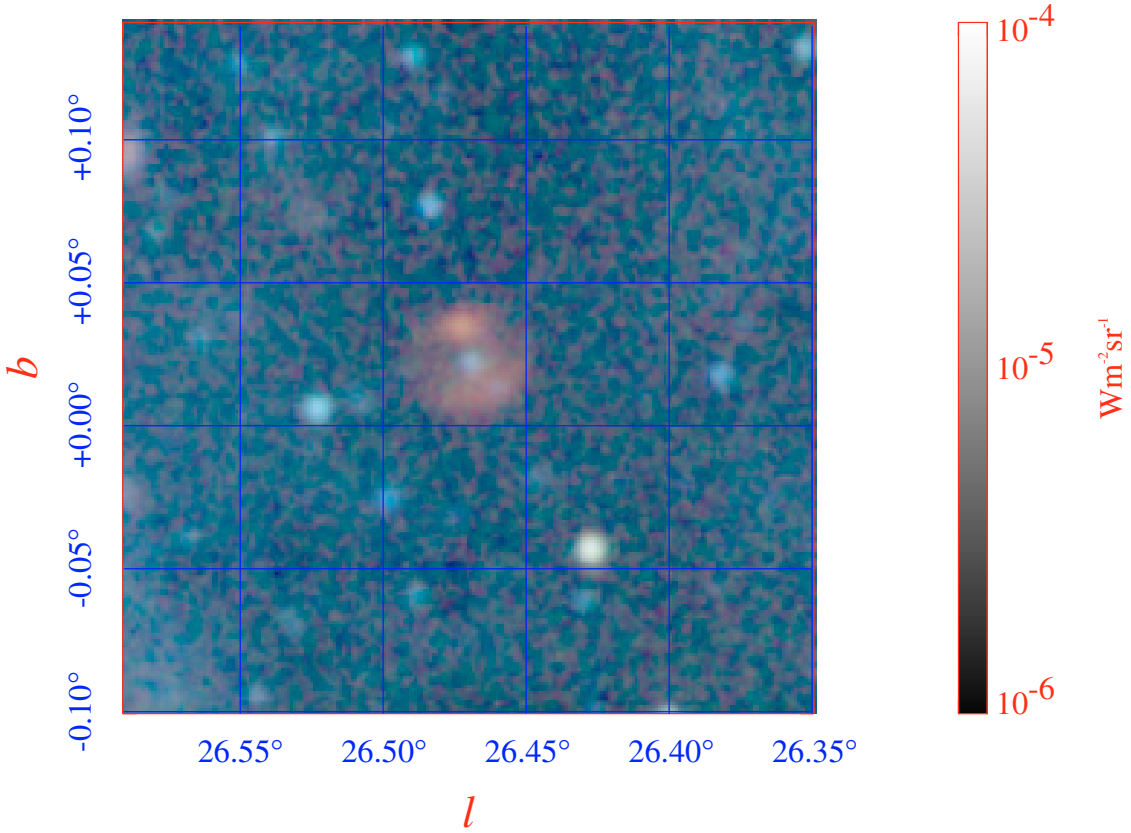

Fig. 4. Three colour image of G26.47+0.02 from MSX. *Blue*: Band *A* (6.8–10.8 μm); *green*: bands *C* and *D* (11.1–15.9 μm); *red*: Band *E* (18.2–25.1 μm). The field of view of the figure is 0.3° × 0.3°.

Table 2. Broad band *JHK* photometry for G24.73+0.69 and G26.47+0.02 obtained during 2001–2002 from the AZT-24 1.1 m telescope at Campo Imperatore. Archival 2 mass survey data obtained in the period between 1997–2001 are also presented for both objects.

Star	Date	*J*	*H*	*K*
G24.73+0.69	2 mass	8.36 ± 0.02	6.84 ± 0.04	5.92 ± 0.02
	2001 March 18	8.28 ± 0.02	6.85 ± 0.02	6.23 ± 0.02
	2001 March 23	8.20 ± 0.02	6.78 ± 0.02	6.15 ± 0.02
	2001 Sep. 20	8.07 ± 0.02	–	–
	2002 April 25	8.32 ± 0.02	–	–
	2002 April 27	8.32 ± 0.02	6.82 ± 0.02	6.04 ± 0.02
	2002 May 15	8.22 ± 0.02	6.71 ± 0.02	5.95 ± 0.02
	2002 July 18	8.10 ± 0.02	6.61 ± 0.02	5.85 ± 0.02
	2002 August 2	8.06 ± 0.02	6.59 ± 0.02	5.89 ± 0.02
	2002 August 14	8.07 ± 0.02	6.60 ± 0.02	5.87 ± 0.02
G26.47+0.02	2 mass	8.00 ± 0.02	6.53 ± 0.02	5.61 ± 0.02
	2001 April 1	8.51 ± 0.05	7.07 ± 0.05	6.07 ± 0.05
	2002 April 27	8.38 ± 0.02	6.96 ± 0.02	5.76 ± 0.02
	2002 July 18	8.47 ± 0.02	7.04 ± 0.02	5.95 ± 0.02
	2002 August 2	8.50 ± 0.02	7.06 ± 0.02	5.96 ± 0.02
	2002 August 14	8.47 ± 0.02	7.04 ± 0.02	5.89 ± 0.02

4. Radio observations

No radio sources are found to be associated with G24.73+0.69; however radio emission is found to be associated with G26.47+0.02. Becker et al. (1994) report two resolved radio sources within the boundaries defined by the MSX nebula (Table 3), while the NVSS survey (Condon et al. 1998) reveals a marginally resolved (45″) radio source ($S_{1.4\ \mathrm{GHz}}$ = 84.5 mJy) ∼ 6″ away from the position of the central object derived from the MSX data. Therefore, while G26.47+0.02 appears to be a radio source, the large scale nebular structure appears to be resolved out by the baselines used in the observations presented by Becker et al. (1994), making an accurate

Table 3. Source positions (J2000), peak and integrated 5 and 1.4 GHz fluxes and sizes for the 2 radio sources within the confines of the G26.47+0.02 nebula (Becker et al. 1994).

Source	RA	Dec	$S_{\rm peak}$	$S_{\rm integrated}$ 5GHz	diam.	$S_{\rm peak}$	$S_{\rm integrated}$ 1.4GHz	diam.
GPSR26.470+0.025	18 39 31.5	−05 44 12.6	4.5 mJy	19 mJy	8.1″	8 mJy	23 mJy	6.7″
GPSR26.470+0.021	18 39 32.2	−05 44 19.6	29.8 mJy	41.4 mJy	2.8″	12 mJy	17 mJy	3.3″

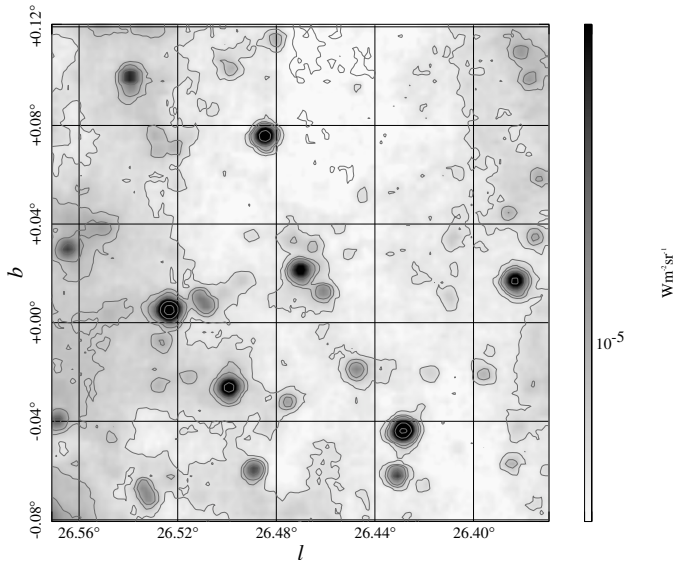

Fig. 5. Image and contours of MSX band A (8.3 μm) data for G26.47+0.02. Contour levels are 0.55, 0.70, 0.85, 1.0, 1.5, 3 and 5 × 10^{-5} Wm^{-2} sr^{-1} and the image stretch is logarithmic between 6.0 × 10^{-6} and 2.5 × 10^{-5}.

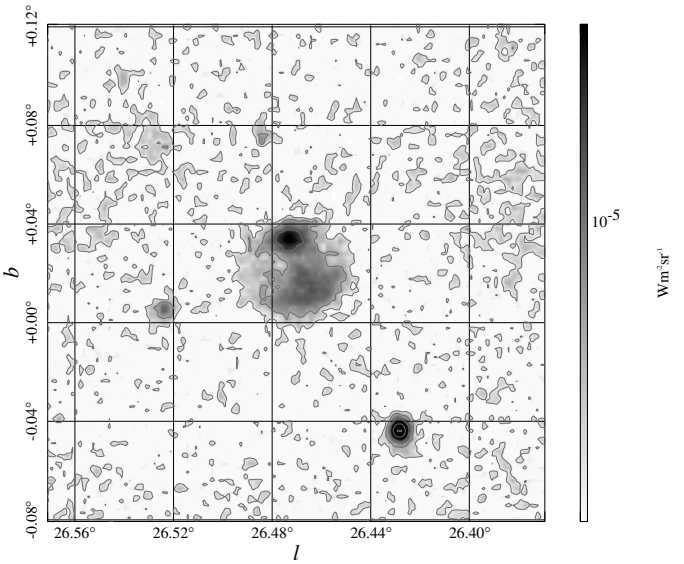

Fig. 6. Image and contours of MSX band E (21.34 μm) data for G26.47+0.02. Contour levels are 0.3, 0.6, 1.5, 3, 4.5, 9 and 15 × 10^{-5} Wm^{-2} sr^{-1} and the image stretch is logarithmic between 2.5 × 10^{-6} and 2.5 × 10^{-5}.

determination of integrated flux (and hence spectral index) impossible from the present observations.

5. IR spectroscopy

Near–IR spectroscopic observations of G24.73+0.69 and G26.47+0.02 were made in service time with the United Kingdom Infrared Telescope (UKIRT) on 2001 June 16–17 and 2002 August 6 using the Cooled Grating Spectrometer (CGS4). Observations between 2.0–2.5 μm were made using the long focal length camera plus the 40 line/mm grating, resulting in a resolving power of 800. 2× oversampling was employed. Standard throws along the slit to maximise the S/N were employed for G24.73+0.69; however given the possibility of significant line emission from the ionised gas associated with G24.73+0.69 (as indicated by the presence of strong radio emission), we chopped to a position 180″ away in declination in order to avoid nebular contamination.

Initial data reduction was carried out at the telescope using the ORACDR software package. This removes bad pixels, debiases, flat-fields, linearity corrects and interleaves oversampled scan positions. The subsequent stages of data reduction, comprising of sky subtraction, extraction, derippling and wavelength calibration using observations of a CuAr lamp, were carried out using the Starlink-supported package FIGARO. The resultant spectra are presented in Fig. 10.

These spectra were supplemented by lower resolution ($R \sim$ 270) observations made on 2002 May 13, May 26 and July 22 from the AZT-24 1.1 m telescope, with the IR imaging camera SWICAM and the IJ and HK band grisms. These provided spectral coverage between 0.84–1.32 μm and 1.45–2.38 μm respectively, and are presented in Fig. 11.

Measurement of the centroids and equivalent widths (EW) of the emission lines in all spectra was accomplished with DIPSO; these are presented in Tables 4 and 5.

We find that the spectra of both stars are dominated by pronounced H I, He I and low excitation metallic (Fe II and Mg II) emission. Na I emission is also apparent in the CGS4 spectra of both stars. No emission is observed in transitions of high excitation species (such as He II, C III and IV and N III) that are found in this wavelength range in the spectra of O stars and Wolf Rayets. Likewise, no molecular or atomic photospheric features – as might be expected for cool luminous stars – are present; the lack of Si II 2.180 μm absorption line implying temperatures of >10 000 K for example.

Within the observational uncertainties no spectral variability is found for G26.47+0.02 (Table 5). Comparison of the 2001 and 2002 spectra of G24.73+0.69 suggests a possible reduction in strength of the He I 2.058 μm, Fe II 2.089 μm and Brγ transitions accompanied by a strengthening of Na I 2.206/9 μm. Note that G24.73+0.69 also appears photometrically variable ($\Delta JHK = 0.3$ mag) during this time.

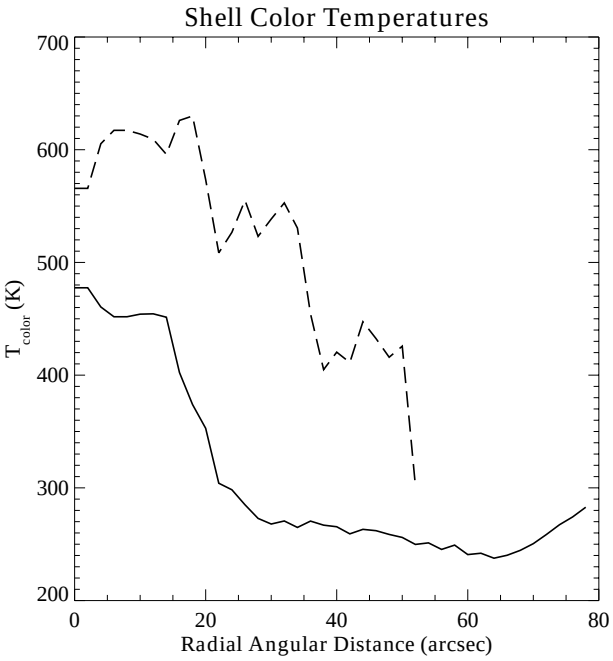

Fig. 7. Plot of the shell colour temperature for G24.73+0.69 (dashed line) and G26.47+0.02 (solid line) as a function of radial distance.

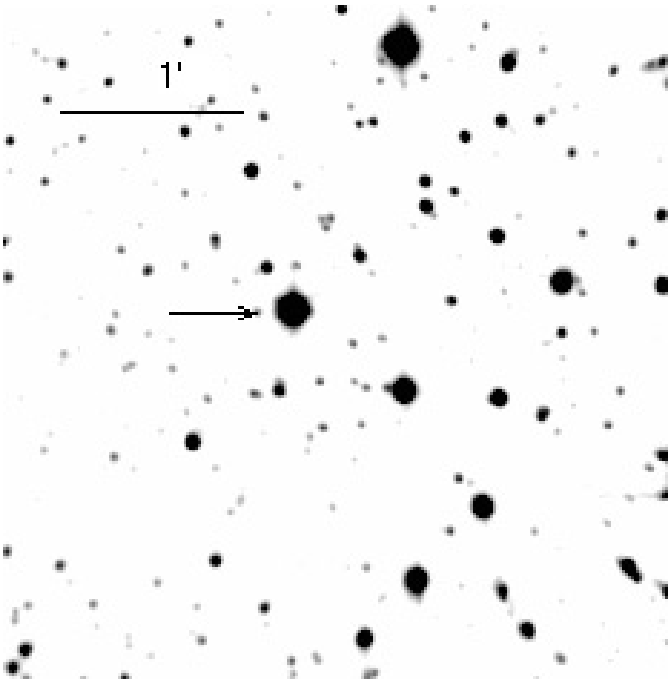

Fig. 8. *K* band image of the field surrounding G24.73+0.69. The field is ∼4′ square, and the IR counterpart to the central MSX point source is the bright object indicated with an arrow.

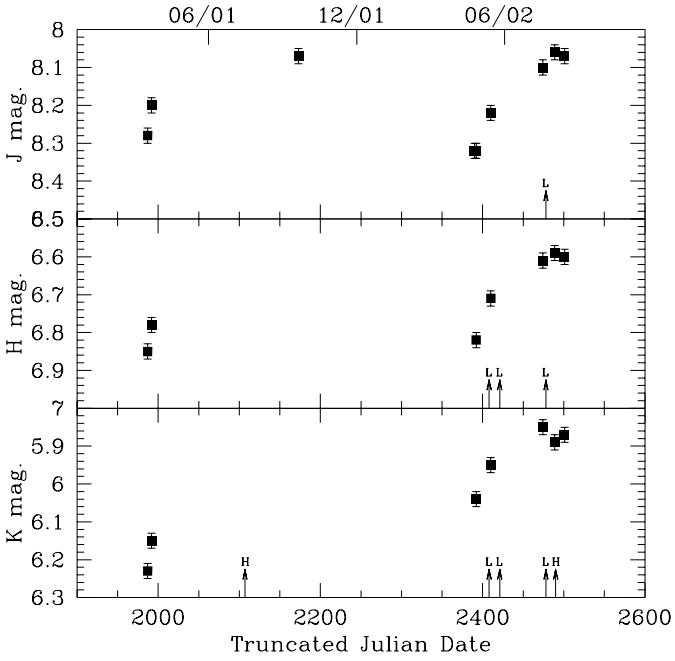

Fig. 9. JHK broadband photometry of G24.73+0.69. The date spectra were taken is indicated by an arrow and resolution by either **L**ow or **H**igh.

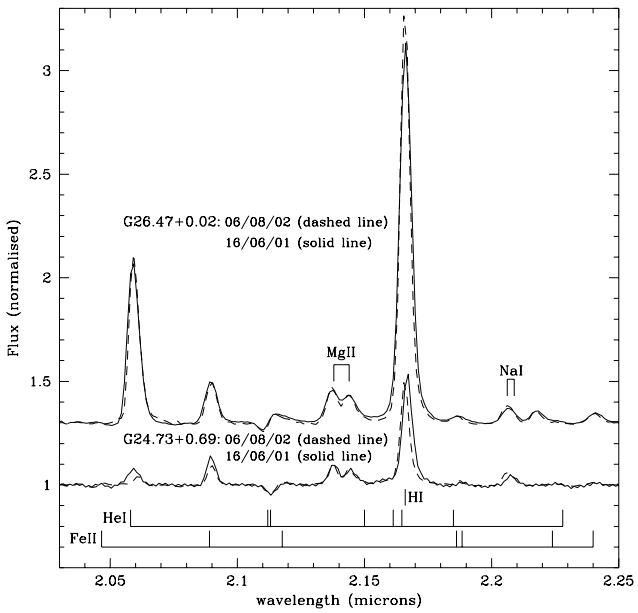

Fig. 10. CGS4 *K* band spectra of G24.73+0.69 and G26.47+0.02 between 2001–02 with major transitions indicated.

6. Discussion

6.1. The central stars

Spectral classification of significantly reddened stars is somewhat problematic, given the inaccesibility of the blue end of the optical spectrum (∼4000 Å) typically used to classify early stars. Fortunately a number of studies of massive main sequence, transitional and Wolf Rayet stars in the near-IR (∼1–3 μm) have been published over the last decade, typically enabling classification of stars to within ±2 spectral types. However, even a cursory examination of the spectra reveals a close affinity with the spectra of other (c)LBVs and B[e] stars (e.g. Morris et al. 1996; Voors et al. 2000b and Egan et al. 2002; Sect. 6.3.1).

In order to determine the stellar parameters of both objects we have computed a series of B supergiant models using the Hillier & Miller (1998) line blanketed, non-LTE model atmospheric code. A major difficulty with this work is the

Table 4. Line identification, wavelengths (given in μm) and equivalent widths (*EW*; given in Å) between ∼0.9–1.8 μm for G24.73+0.69 and G26.47+0.02 We estimate errors to be ±20 per cent for lines between ∼1.5–1.8 μm and ±10 per cent shortwards of this. Note that within the observational uncertainty none of the sources appeared variable over the 3.5 month period of observations – hence we present an average *EW* for each transition.

Star		G24.73+0.69	G26.47+0.02
Transition	λ		
Pa9	0.930	n/a	65
Pa8	0.955	n/a	58
Fe II($z^4F_9 - b^4G_{11}$)+	1.000	bl	bl
Pa7	1.005	66	90
Fe II blend	∼1.05	–	30
He I($2s^3S - 2pb^3P^0$)	1.083	bl	120
Paγ	1.094	45	110
Fe II($z^4F_3 - b^4G_5$)	1.113	–	15
N I	1.246	–	25
Paβ	1.282	42	170
Br16	1.556	–	4
Br15	1.570	–	8
Br14	1.588	–	11
Br13	1.611	8	16
Br12	1.641	13	22
Fe II($z^4F_9 - c^4F_7$)+	1.679	bl	bl
Br11	1.681	38	50
Br10	1.736	28	44

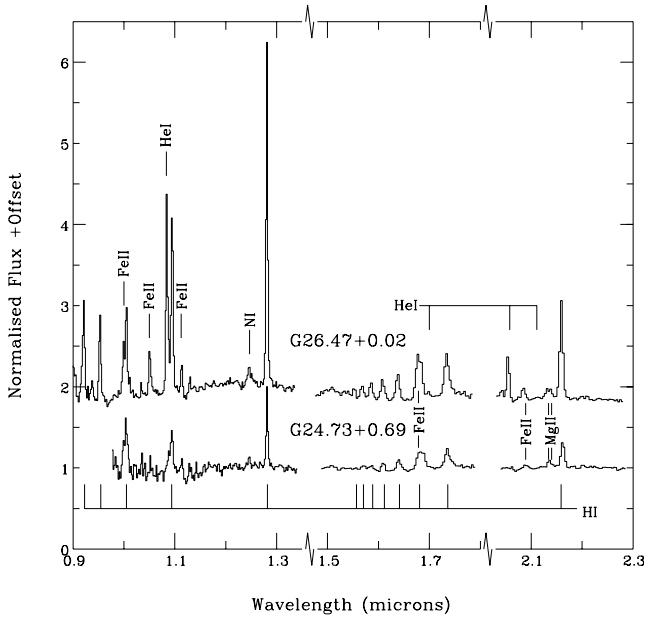

Fig. 11. Low resolution *IJ* and *HK* band spectra of G24.73+0.69 and G26.47+0.02. Both spectra are dominated by emission from H I, He I and low excitation metals such as Fe II.

determination of accurate distances for both objects. Such a task is particularly problematic for galactic field B supergiants, given both the lack of luminosity diagnostics in their spectra and, for the wavelength range in question, the absence of Diffuse Interstellar Bands, from which an estimation of the interstellar reddening might be obtained. Given the inherent uncertainty in any estimate, we choose to quote a *maximum* distance to each object based on consistency between the model and dereddened near-IR spectral energy distribution. We find $E(B-V) = 3.4$ and 3.8 for G24.73+0.69 and G26.47+0.02 respectively, which, assuming an average $A_v = 1.8$ mag kpc^{-1} (Whittet 1992; cf. Wra 17-96, Egan et al. 2002), imply maximum distances of 5.2 and 6.5 kpc. For changes in distance by factors of ≤2, the proportionalities given for the luminous B supergiant HD 316285 (Hillier et al. 1998) may be used to scale the stellar parameters of both objects given below.

For the derivation of stellar parameters, model calculations were carried out using similar atomic datasets and elements to that undertaken by Drissen et al. (2001) for NGC2363-V1. In total, the following ionization stages were considered: H I, He I–II, C II, N I–II, O I–II, Na I, Mg I–II, Al II–III, Si II–III, S II–III, Cr II–III, Fe II–III and Ni II–III. Solar abundances were adopted throughout, with the exception of helium (see later). Unfortunately, given the narrow wavelength range and intermediate resolution of the CGS4 observations, we were forced to adopt a terminal wind velocity (200 km s^{-1}) for both objects (cf. AFGL 2298; Clark et al. 2003). Note that charge exchange, important for many Fe II transitions, was accounted for following Hillier et al. (2001). Line blanketing was treated using a global Doppler line width of 10 km s^{-1}, whilst wind clumping was neglected. Stellar parameters were then determined by simultaneously reproducing the Brγ, He I+ Fe II 2.058 μm and Fe II 2.09 μm emission profiles, together with contemporaneous broad band photometry. Finally, for G24.73+0.69, an enriched H/He abundance of 5 by number – typical of Luminous Blue Variables during mid-B evolutionary phase (Crowther 1997) – was adopted. However, for G26.47+0.02 the optimal fit was obtained using *solar* H/He abundances, implying a less evolved surface chemistry for this object.

Despite the caveats arising from the limited diagnostics and uncertain distances, best fit stellar parameters for both sources are presented in Table 6 and synthetic spectra, degraded to the resolution of the CGS4 spectra, are plotted in Fig. 12. Both objects appear to be luminous B supergiants with high mass loss rates. Indeed, with $\dot{M} = 9\times10^{-5}\ M_\odot$ yr^{-1} G26.47+0.02 has one of the highest mass loss rates of any known BSG or LBV (e.g. Clark et al. 2003).

As such, they appear similar to, and occupy a region of the HR diagram populated by, other (c)LBVs; an issue that will be returned to in Sect. 6.3.1. We note in passing our inability to reproduce the Na I emission in both objects, despite the inclusion of sodium in the models. The physical process leading to this discrepancy is at present unclear; however the presence of Na I emission, which is absent for the hotter Ofpe/WN9 stars (Bohannan & Crowther 1999), confirms the relatively low temperature found for both objects (cf. AFGL 2298; Clark et al. 2003).

6.2. The Mid-IR ring nebulae

To determine the true dust shell parameters and constrain the mass loss history of both sources, we have modeled the

Table 5. Line identifications (wavelengths given in μm) from K band (~2–2.35 μm) spectra for G24.73+0.69 and G26.47+0.02 Note that we have adopted the convention that emission lines are quoted as positive throughout the table. We estimate errors of ±10 per cent for the UKIRT spectra and ±20 per cent for the spectra from Campo Imperatore. Note that within the observational uncertainties the *EW* measured from the 3 low resolution spectra taken between 2002 May–July are identical to one another; hence we only quote a mean value.

Star		G24.73+0.69			G26.47+0.02		
Date		16/06/01	05–07/02	06/08/02	16/06/01	05–07/02	06/08/02
Transition	λ		*EW*(Å)			*EW*(Å)	
He I ($2s^1S - 2p^1P^0$)	2.058	5.0	–	1.7	43.0	35	45.0
Fe II ($z^4F_{3/2} - c^4F_{3/2}$)	2.091	6.2	–	4.0	11.4	11	11.2
He I ($3p^3P^0 - 4s^3S$)	2.112	–1.4	–	–1.4	–0.9	–	–0.8
+ He I ($3p^1P^0 - 4s^1S$)	2.113	bl	–	bl	bl	–	bl
Fe II ($c^4P^0_{3/2} - z^4D^0_{5/2}$)	2.118	–	–	–	2.0	–	1.8
Mg II ($5s^2S_{1/2} - 5p^2P^0_{1/2}$)	2.138	4.7	6	4.1	9.4	14	10.1
Mg II ($5s^2S_{1/2} - 5p^2P^0_{1/2}$)	2.144	3.4	bl	3.3	5.1	bl	5.3
He I ($4p^3P - 7s^3S$)	2.150	–	–	–	–	–	–
Brγ	2.166	28.0	26	22.0	104.0	90	100.0
He I ($4p^1P$ - $7d^1D$)	2.185	0.6	–	0.7	1.8	–	1.7
Na I ($4p^2\ P^0_{3/2} - 4s^2S_{1/2}$)	2.206	2.4	–	3.4	3.9	–	5.4
+Na I($4p^2\ P^0_{3/2} - 4s^2S_{1/2}$)	2.209	bl	–	bl	bl	–	bl
Fe II($a^4P_{1/2} - a^2P_{3/2}$)	2.244	–	–	–	3.6	–	3.1

Table 6. Stellar parameters of G24.73+0.69 and G26.47+0.02, derived from comparison of the spectrosocopic and photometric datasets to NLTE synthetic spectra (see Sect. 3 for details). Note that $v_{\rm exp}$ cannot be determined directly from the present dataset and hence was set to a value appropriate for a high luminosity mid-B supergiant.

Parameter	G24.73+0.69	G26.47+0.02
$v_{\rm exp}$ (km s^{-1})	200	200
H/He	5	10
$T_{\rm eff}$ (kK)	12	17
log ($\dot{M}$) ($M_\odot$ yr^{-1})	−5.00	−4.05
$E(B-V)$	3.4	3.8
Dist. (kpc)	≤5.25	≤6.5
log($L_*/L_\odot$)	≤5.6	≤6.0
R_* ($R_\odot$)	≤115	≤ 146

observations using a modified version of the radiative transfer code of Egan et al. (1988), following the methodology described in Egan et al. (2002) for Wray 17-96. As in the Wray 17-96 models, we have concentrated here on fitting the radiance of the extended IR ring nebula, paying less attention to fitting the details of the central source emission. As noted previously, the colour of the central source, and the evidence for large contemporaneous mass loss rates indicate that we cannot expect a stellar photosphere to accurately model the infrared measurements of the central source. We expect that free–free and/or hot dust emission to account for a substantial fraction of the emission within 20″ of the source position. Because the photospheric emission of the star can only account for less than half of the observed mid-IR radiance of G24.73+0.69 and G26.47+0.02, we have added a free–free emission term,

$$I_{\rm ff}(\nu) = A \exp(h\nu/kT_{\rm e}), \quad (1)$$

to the blackbody radiation intensity of the central star. For G24.73+0.69 we have set $A = 1.5 \times 10^{-16}$ ergs cm^{-2} s^{-1} Hz^{-1} sr^{-1}, and $T_{\rm e} = 10\,000$ K. For

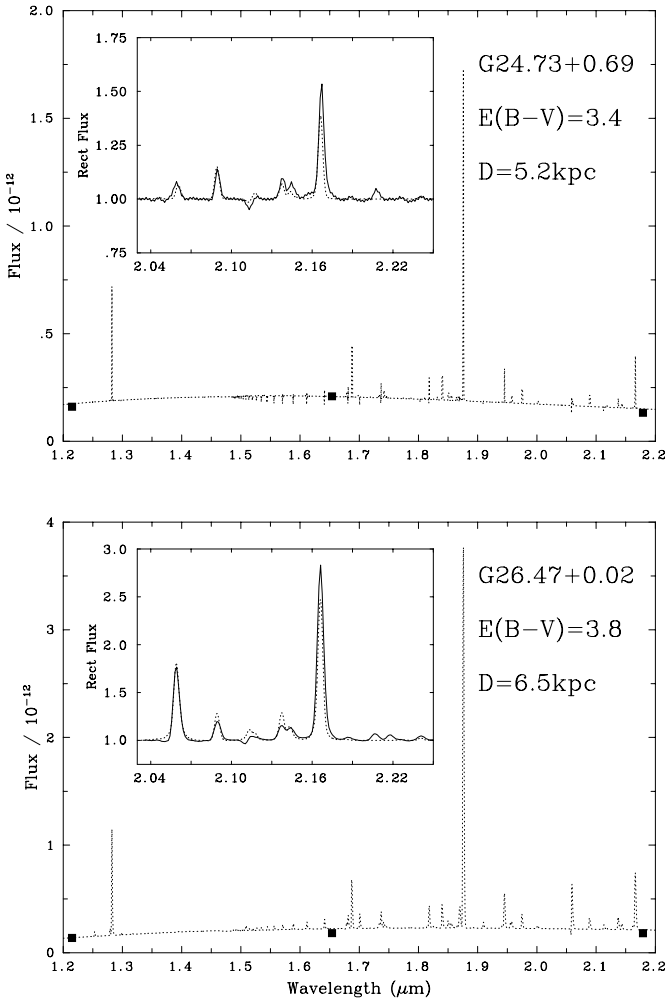

Fig. 12. Upper panel: comparison of reddened spectral energy distribution of G24.73+0.69 (dotted line) to broad-band *JHK* photometry (squares), plus rectified synthetic spectra (dotted line), degraded to the CGS4 resolution, compared to UKIRT spectroscopy. Lower panel: As above for G26.47+0.02.

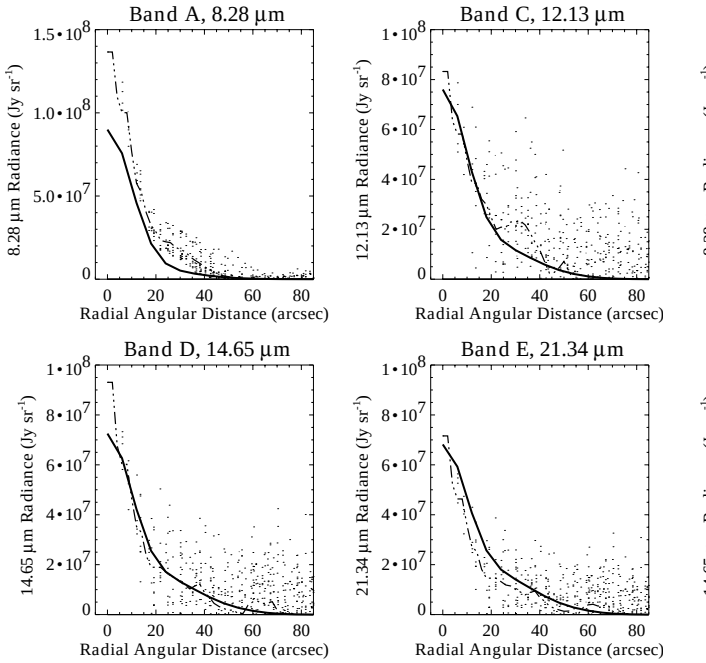

Fig. 13. Radiative transfer model results for G24.73+0.69 in the 4 MSX IR Bands (solid line). The points show the MSX image pixel values (radially from stellar position), with the dotted lines denoting the average observed intensity (averaged over the ±3″ nearest each sample point).

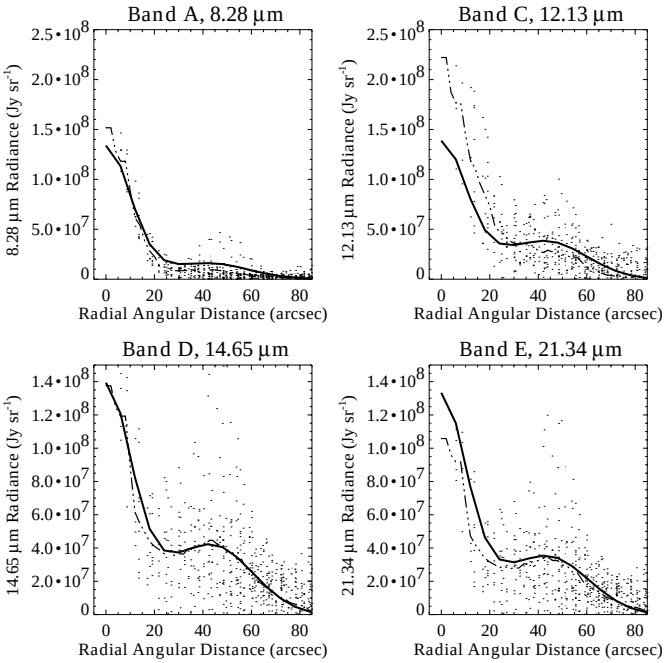

Fig. 14. Radiative transfer model results for G26.47+0.02 in the 4 MSX IR Bands (solid line). The points show the MSX image pixel values (radially from stellar position), with the dotted lines denoting the average observed intensity (averaged over the ±3″ nearest each sample point).

Table 7. Best fit nebular model paramters for G24.73+0.69 and G26.47+0.02 (central source characteristics from Table 6). The ratio by number of silicate:iron grains for G24.73+0.69 and G26.47+0.02 is 50:50 and 33:67, and by mass 85:15 and 74:26, respectively. Note we assume a gas:dust ratio of 100:1 for the calculation of the total nebular mass.

	G24.73+0.69	G26.47+0.02
τ (0.55 μm)	3.06×10^{-4}	4.68×10^{-4}
τ (8.28 μm)	1.0×10^{-4}	1.05×10^{-4}
$R_{\rm in}$ (pc)	0.66	1.40
ΔR(pc)	0.97	0.97
$a^{\rm silicate}(\mu{\rm m})$	0.01	0.01
$T_{\rm in}^{\rm silicate}$ (K)	61	59
$M_{\rm dust}^{\rm silicate}$ ($M_\odot$)	3.83×10^{-3}	0.014
$a^{\rm Fe}(\mu{\rm m})$	0.005	0.005
$T_{\rm in}^{\rm Fe}$ (K)	189	189
$M_{\rm dust}^{\rm Fe}$ ($M_\odot$)	6.75×10^{-4}	4.94×10^{-3}
$M_{\rm dust}^{\rm total}$ ($M_\odot$)	0.0045	0.019
$M_{\rm tot}$ ($M_\odot$)	0.45	1.9

G26.47+0.02, $A = 1.1 \times 10^{-16}$ ergs cm^{-2} s^{-1} Hz^{-1} sr^{-1}, and $T_{\rm e} = 15\,000$ K. While these terms do allow us to better fit the mid-IR radiance within 20″ of the central source – and are consistent with the results of the stellar modeling in Sect. 6.1 – their inclusion does not alter the radiance of the extended IR nebula; hence the results presented below – and the conclusions of Sect. 6.4.2. – remain unaffected. This is because the heating of the dust in the extended shell is dominated by UV and visible radiation from the central star, which still dominates over the free–free emission.

The best fit parameters for the dust shell are given in Table 7, and the integrated radial intensity overplotted on each dataset is shown in Figs. 13 and 14. In both cases we were able to fit the extended IR nebula with a single geometrically thick (∼1 pc) shell with a r^{-2} density gradient. As for Wray 17-96, we were unable to fit either G24.73+0.69 or G26.47+0.02 with a pure silicate or carbonaceous dust shell. The best fits were provided by shells composed of a mixture of silicate (Mg_2SiO_4; optical constants from Jager et al. 1998) grains ($a = 0.01$ μm) and small ($a = 0.005$ μm) warmer Fe grains (optical constants from Pollack et al. 1994). The warm Fe grains are required to match the observed shell colors – pure silicate grains yield too little radiance in the shorter wavelength MSX bands. The fraction by mass of both dust components are given in Table 7. Both populations are co-spatial and in thermal equilibrium with the stellar radiation field. It would also have been possible to match the observed colors by using a combination of silicate and carbonaceous grains in the dust shell. While there is evidence in many (c)LBVs of mixed O-rich and C-rich dust (e.g. Egan et al. 2002; and references therein), there is a presumption based on stellar evolution theory against mixed oxygen and carbon chemistry. Therefore we have attempted to model both G24.73+0.69 and G26.47+0.02 using only dust components consistent with an O-rich chemistry. This model works quite well for G26.47+0.02, while for G24.73+0.69 we still cannot produce enough flux in the MSX Band *A*, similar to the problems found in our modeling of Wray 17-96. This may be evidence of either emission from aromatic hydrocarbons, nonthermal small grain emission, or another warm dust shell interior to the shell we have modeled.

Table 8. Duration of nebular formation and inferred mass loss rate for both sources, assuming a wind velocity of 200 km s^{-1}. Adopting a lower velocity of 20 km s^{-1} (appropiate for a RSG) increase timescales by an order of magnitude, and reduces the requisite mass loss rate by the same amount. For comparison, present day mass loss rates for G24.73+0.69 and G26.47+0.02 are 10^{-5} and 9×10^{-5} $M_{\odot}$ yr^{-1} respectively.

Mass Loss	G24.73+0.69	G26.47+0.02
Onset (yr)	−8000	−11 660
Cessation (yr)	−3200	−6860
Age (yr)	4800	4800
$\dot{M}$ ($M_{\odot}$ yr^{-1})	9.5×10^{-5}	4.0×10^{-4}

Finally, we present the inferred ages of the nebulae in Table 8, adopting an expansion velocity of 200 km s^{-1} during the ejection event (appropiate for a BSG; Sect. 6.1). For both objects we find that the nebulae are rather young, and the requisite mass loss rates for their formation are less than an order of magnitude greater than those inferred from the present data.

Alternatively, an expansion velocity of 20 km s^{-1} (appropiate for a RSG) results in a mass loss rate *less* than that observed at present for both objects. Consequently, we consider such a low wind expansion velocity during nebular formation unlikely. Additionally, such a velocity implies an age of ∼60 000 yrs for the G26.47+0.02 nebula. Assuming formation in a post-MS, pre-WR phase, the rapidity with which massive stars are expected to evolve into H depleted WN objects (e.g. ∼25 000 yrs for the LBV phase; Voors et al. 2000a) presents difficulties for a formation scenario invoking a low wind velocity, given that the surface abundances of G26.47+0.02 show no signs of chemical enrichment.

6.3. The outer shell of G24.73+0.69

As noted in Sect. 2, a second larger, fragmentary shell appears associated with G24.73+0.69. At a distance of ∼5 kpc (Sect. 6.1), we find the dimensions of the semi-major and -minor axis to be $\sim(7.25 \times 3.6)\cos(\theta)$ pc (where θ is the angle between the major axis and the plane of the sky). Adopting an expansion velocity of ∼200 km s^{-1} (cf. Sect. 6.1) implies a minimum age of ∼36 000 yrs for this structure.

Such a size and inferred age makes it unlikely that the emission originates in material ejected from G24.73+0.69 during an LBV phase (cf. Sect. 6.4.2 and Table 9). Instead we believe it is more likely to be due to the interaction of the stellar wind and surrounding ISM or natal cloud, with the emission from polycyclic aromatic hydrocarbons (PAHs) in photodissociation regions on the interface between wind and ambient medium. We note however that Meaburn et al. (1999) associate a similarly extended ($\sim 3.7\cos(\theta)$ pc) lobe of nebular emission with the LBV P Cygni. While they too discount an origin in the current phase of LBV activity, they conclude that the emission originates in material ejected – via an as yet unspecified mechanism – by P Cygni, rather than in an interaction between stellar wind and the ISM.

6.4. Comparison to (c)LBV

6.4.1. The central stars

A key question regarding the ring nebulae sources presented in this work – G24.73+0.69 and G26.47+0.02 – and those in Egan et al. (2002) – Wra 17-96 and G79.29+0.46 – is their relationship to the diverse family of massive post-MS objects. A cursory examination of the K band spectra of these objects (a spectrum of G79.29+0.46 is presented by Voors et al. 2000b) reveals that they clearly form a homogeneous group of highly luminous B supergiants. To this putative class of object we might also include AFGL 2298 (Clark et al. 2003), for which the large distance (∼10 kpc) and intrinsically compact nebula (Ueta et al. 2001) prevents its complete resolution by MSX and the Pistol Star, for which a (distorted) ring nebula is visible in both MSX (Crowther & Conti, in prep.) and ISOCAM observations (Moneti et al. 1999).

Of immediate interest is the close similarity between the K band spectra of these objects and those of the bona fide LBVs Wra 751 and AG Car (Voors et al. 2000b). Since only the limited spatial resolution of MSX prevents us from resolving the dusty ring nebulae surrounding these 2 LBVs (Voors et al. 2000a), do the 6 MSX ring nebulae sources exhibit the characteristic variablity of LBVs?

Both AFGL 2298 (Clark et al. 2003) and the Pistol Star (Glass et al. 1998; Figer et al. 1998) demonstrate significant photometric ($\Delta K \geq 0.5$ mag) and spectroscopic variability, immediately suggesting LBV classifications. Despite a limited baseline of observations, G79.29+0.46 also appears to show "significant spectroscopic variability" (Krauss et al. 2000) while we show here that G24.73+0.69 is photometrically (and probably spectroscopically) variable. Of the two remaining sources only one epoch of observations exist for Wra 17-96 while comparison of our data to the 2 mass results for G26.47+0.02 are at least suggestive of photometric variability – clearly both sources could yet demonstrate the characteristic variability of LBVs.

Indeed, with the exception of the unusual cLBV G25.5+0.2 – which apppears to have a much hotter pseudo-O star spectrum (Clark et al. 2000) – we find a remarkably close correspondance between the (c)LBVs and the central objects of MSX ring nebulae; a notable example being FMM 362 in the Quintuplet Cluster (Geballe et al. 2000)[2].

However, while comparisons based on spectral *morphologies* are suggestive of a link between the MSX ring nebulae sources and the LBVs, quantitative analysis (and long term monitoring) will be required to establish a direct correspondance. For instance we should like to determine if differences in properties such as metallicity and mass loss rates exist between these two classes of objects and also the sgB[e] stars HD 72754 and S18, which, despite sharing similar spectral morphologies (Morris et al. 1996), demonstrate neither the characteristic variability of LBVs, nor are associated with ejection nebulae.

[2] Glass et al. (1998) show FMM 362 to be variable with a peak to peak K band intensity of 0.92 ± 0.06 mag, and hence an LBV.

Table 9. Stellar luminosities, nebular radii and dust and gas masses for known (upper panel), cLBV (middle panel) and the MSX ring nebulae sources (lower panel). Where total nebular masses are inferred from dust masses we have assumed a standard 100:1 gas:dust ratio; such values are indicated by italics. Note that on the basis of the large magnitude photometric and spectroscopic variability we consider AFGL 2298 a bona fide LBV, and while the Pistol Star is almost certainly an LBV (Sect. 6.3.1 and Refs. therein) we still opt (conservatively) to consider it a cLBV (cf. van Genderen 2001). Mid-IR observations reveal that many nebulae have significant geometric thicknesses – where appropiate the inner and outer radii are indicated (denoted by an arrow), as are the dimensions of the major and minor axis of those sources which deviate from circular symmetry. [1] Dust mass for HD 168625 has been scaled to a distance of 2.8 kpc. [2] Subrahmanyan et al. (1994) assume $T_{\rm eff}$ = 34 kK; however Clark et al. (2000) show that G25.5+0.2 is likely to be significantly hotter, thus the quoted luminosity is a lower limit. $M_{\rm gas}$ derived from radio fluxes is dependant on the value adopted for the uncertain filling factor f; adopting $f \sim 0.2$ leading to $M_{\rm gas} \sim 5.4\ M_{\odot}$ (Subrahmanyan et al. 1994). References for table entries are [a] Hillier et al. (2001), [b] Morris et al. (1999), [c] Voors et al. (2000b), [d] Voors et al. (1997), [e] White (2000), [f] Nota et al. (1995), [g] Smith et al. (1994), [h] Pasqualli et al. (2002), [i] Robberto & Herbst (1998), [j] Lamers et al. (2001), [k] Meaburn et al. (2000), [l] Ueta et al. (2001), [m] Clark et al. (2003), [n] Schulte-Ladbeck, in prep., [o] Voors et al. (1999), [p] Figer et al. (1999), [q] Moneti et al. (1999), [r] Subrahmanyan et al. (1994), [s] Clark et al. (2000), [t] Hutsemekers (1997), [u] Pasquali (1997), [v] Higgs et al. (1994), [w] Voors et al. (2000a), [x] Egan et al. (2002).

Star	$\log(L/L_{\odot})$	$R_{\rm neb}$ (pc)	$M_{\rm dust}$ ($M_{\odot}$)	$M_{\rm gas}$ ($M_{\odot}$)
η Car[a,b]	6.7	0.1	0.15	3–15
AG Car[c]	6.25	0.36→0.80	0.22	8.9
HR Car[d,e,f]	5.7	0.26	$<8 \times 10^{-4}$	0.8–2.1
Hen 3-519[g]	5.7	1.14	0.007	2.0
Wra 751[c]	5.7	0.17→0.34	0.017	1.7
HD 168625[1,h,i]	5.6	0.21 × 0.24	0.016	2.1
P Cyg[j,k]	5.8	0.4	0	0.01
AFGL 2298[l,m]	6.2	0.12→0.72	0.1	*10*
R 127[j,n]	6.1	1.05 × 0.8	–	10 ± 2
S 119[j,n]	6.0	1.0 × 0.9	–	2.6 ± 0.7
R 71[o]	5.85	0.12→0.18	0.02	*2*
Pistol Star[p,q]	6.6	1.5	0.004	11
G25.5+0.2[2,r,s,t]	>5.9	0.4 × 0.6	>0.06	5.4
S 61[j,u]	6.1	0.7 × 0.65	–	14 ± 3
G79.49+0.26[v,w]	5.5	0.8→3.6	0.15	15
Wra 17-96[x]	6.26	0.7→2.2	0.1	*10*
G24.73+0.69	5.6	0.7→1.7	0.0045	*0.45*
G26.47+0.02	6.0	1.4→2.4	0.019	*1.9*

6.4.2. The ejection nebulae

Given the apparent close correspondance between the central stars of the MSX ring nebulae and the bona fide LBVs it is instructive to compare the properties of the nebulae of both classes of object, which we summarise in Table 9. We emphasise that several difficulties exist with collating data for such a comparison however. Determination of nebular radii is non trivial, given that measurements from optical or radio and mid-IR observation can yield different results (e.g. Wra-751; Voors et al. 2000a). Where there is conflict we adopt the radii derived from mid-IR measurements to enable direct comparison to the MSX nebulae[3]. Some caution should be exercised over estimates of the outer radius given the difficulty of constraining this parameter from observations typically limited to <25 μm. Likewise, comparison of $M_{\rm dust}$ is prone to difficulties given the differing modeling assumptions made by various authors, with differences in the treatment of grain size distributions (single size or power law), dust emissivity (a simple power law prescription or radiative transfer treatment) and the treatment of scattering all introducing uncertainties[4].

In comparison to the (c)LBVs (Table 9, panels 1 and 2), we find that the *detached* nebulae around G79.49+0.26, Wra 17-96, G24.73+0.69 and G26.47+0.02 have significantly larger inner and outer radii. Undoubtedly, this is at least in part a selection effect based on the minimum angular extent for the nebulae to be resolved by MSX. However, differences may also reflect the fact that we are preferentially sampling cooler, more extended regions of the ejection nebula, with optical and/or radio observations simply detecting ionised material

[3] Note that several sources are assumed to have undergone more than one ejection event – here we simply provide the radii of the inner- and outermost shell.

[4] The lack of long term monitoring data to constrain the evolution of the parameters of the central stars of the nebulae also complicates modeling of the dusty nebular component since the characteristic timescale of LBV variability (and hence stellar temperature) is of the order of the light crossing time for the nebulae.

interior to the bulk of neutral nebular material (cf. Wra 751). Nevertheless, kinematic ages of all sources are $\leq 10^4$ yrs, similar to the proposed lifetime of the LBV phase (based on comparisons between the relative populations of LBVs and WRs; Voors et al. 2000a and references therein).

Evidence for a departure from spherical symmetry is found for the nebulae associated with G79.49+0.26 (Waters et al. 1996), Wra 17-96 (Egan et al. 2002) and G26.47+0.02 (the nebula associated with the Pistol Star appears to have been deformed by interaction with the extreme conditions near the galactic centre). Following the arguments of Ueta et al. (2001) for AFGL 2298, the simplest interpretation of such asymmetries is the presence of a toroidal density enhancement inclined to the line of sight (with the ring around G79.49+0.26, and possibly G24.73+0.69 observed ~face on). As such we find that these nebulae also resemble those of (c)LBVs, which often show a considerable degree of bipolarity.

Surprisingly, considering the similarities in nebular morphologies, we find a wide range of nebular masses for both the MSX ring nebulae sources and the wider population of (c)LBVs (~0.45–15 $M_\odot$; Table 9), with nebular mass apparently *uncorrelated* with stellar luminosity. Furthermore, significant differences exist between the nebular masses of pairs of objects with similar *present day* stellar parameters (e.g. G79.49+0.26 & G24.73+0.69, and G26.47+0.02 & AFGL 2298). While differences in the mass of ionised nebular material might be explained by positing the presence of a significant quantity of neutral material (cf. AG Car), differences in the total dust masses and by extension the total nebular masses inferred appear real (assuming a uniform dust:gas ratio for different objects). This is particularly evident for the nebular masses of the MSX sources (which for Wra 17-96, G24.73+0.69 and G26.47+0.02 were all determined under identical modeling assumptions), which differ by more than an order of magnitude. Moreover, despite the pronounced similarities between the spectra (and hence inferred stellar parameters) of the central objects of the MSX nebulae and the LBV FMM 362, there is *no* evidence for ejecta associated with the latter object.

Related to the differences in nebular masses are the differing radio properties of the MSX sources (Sect. 4) and the (c)LBV; why are some nebulae ionised and detected at radio wavelengths (e.g. White et al. 2000) while others are not? Assuming that a gaseous nebular component is present in those systems without radio nebulae, does this reflect current differences in stellar parameters (e.g. intrinsically low stellar ionising flux or a mass loss rate that is sufficiently high that little ionising flux escapes; cf. HD 316285 Hillier et al. 1998)? Or do the nebulae detected in the radio have a lower density, such that a longer recombination timescale allows them to remain ionised for a greater period of time after a past excursion of the central LBV to a hot, ionising state?

Taken as a whole, these results are suggestive of differences in the mass loss histories of the individual objects. Indeed, significant differences in the time averaged mass loss rates of the (c)LBVs and MSX sources during nebular formation – inferred from ejecta masses and kinematical ages – have been found. These range from $\sim 10^{-4}$ $M_\odot$ yr^{-1} (Wra 751; Voors et al. 2000a and G24.73+0.69; this work) to $\sim 10^{-3}$ $M_\odot$ yr^{-1} (AG Car; Voors et al. 2000a and AFGL 2298; Clark et al. 2003). Additionally, while we find that the mid-IR spectral energy distribution of G26.47+0.02 is consistent with a ~single extended mass ejection event, direct imaging and analysis of the spectral energy distribution of a number of other sources reveal that they have undergone 2 or more discrete mass ejection events (e.g. Wra 17-96 and the Pistol star; Egan et al. 2002 and references therein). Indeed, the nature of the variation of the radial colour temperature of G24.73+0.69 (Fig. 7) and our inability to fit the MSX band *A* fluxes may point to the presence of one or more (warmer) shells interior to the one inferred from the analysis presented in Sect. 6.2.

Such fits to the mid-IR spectral energy distribution further reveal that the majority of sources require the presence of two different dust populations; one consisting of cool, relatively large grains and a second of smaller, warmer grains to provide the requisite flux at ≤ 10 μm. While the mid-IR spectral energy distributions of G79.49+0.26 and G26.47+0.02 appear consistent with a simple O-rich chemistry, other objects, such as Wra 17-96 (Egan et al. 2002) and AFGL 2298 (Ueta et al. 2001) show evidence for a mixed O+C rich chemistry, with the population of small dust grains apparently being composed of C rich material[5].

Therefore, despite the fact that *all* the objects described above share almost identical *K* band spectral morphologies (Sect. 6.4.1) the nebular properties, and mass loss histories inferred from them reveal significant differences between superficially similar stars. While some differences may in part be attributable to a combination of poorly determined observational parameters (most notably distance), others, such as dust chemistries – which may be determined directly from mid-IR observations – appear to reflect fundamental differences between individual objects.

Nevertheless – and despite the above caveats – we are still able to conclude that the range of physical properties inferred for both the central star and ejecta nebulae of the MSX selected objects are *fully consistent* with those of known and candidate LBVs.

7. Conclusions

We have presented comprehensive observational datasets from near-IR to radio wavelengths for two recently discovered MSX ring nebulae sources, G24.73+0.69 and G26.47+0.02. In both cases the nebulae are compact and closely resemble the ring nebulae around the cLBVs G79.49+0.26 and Wra 17-96 (Egan et al. 2002). A second, fragmentary, apparently bipolar nebula of much greater spatial extent is found around G24.73+0.69, and is highly suggestive of the giant lobe associated with the LBV P Cygni (Meaburn et al. 1999).

Near IR photometry of both fields revealed a very red point source at the centre of both MSX nebulae; follow

[5] However, observations at higher spatial *and* wavelength resolution than are provided by the present data are required to fully constrain both the mass loss history and dust chemistry of the MSX ring nebulae sources

up near-IR spectroscopy confirmed their stellar nature. Both spectra are dominated by emission from H I, He I and low excitation metals, suggesting classification as luminous B supergiants. Preliminary modeling of the spectra of both objects confirm this hypothesis. Indeed with $\log(L/L_{\odot}) = 6.0$ and $\dot{M} = 9 \times 10^{-5}\ M_{\odot}\ \mathrm{yr}^{-1}$, G26.47+0.02 appears to be one of the most extreme stars in the galaxy, strikingly similar to the known LBVs AG Car and AFGL 2298.

Radiative transfer modeling of the nebulae suggest they were formed in an extended period of enhanced mass loss from both stars. Assuming an expansion velocity of 200 km s^{-1}, we find a kinematic age of ~5000 yrs for both nebulae, which requires a time averaged mass loss rate less than an order of magnitude higher than presently observed. The spatially resolved mid-IR spectral energy distribution of both nebulae can be adequately described with a single shell composed of O-rich dust. Adopting a gass:dust ratio of 100:1 yields total nebular masses of 0.45 $M_{\odot}$ (G24.73+0.69) and 1.9 $M_{\odot}$ (G26.47+0.02).

Comparison to other MSX sources allows us to identify a homogenous group of B supergiants surrounded by massive dusty envelopes. Intriguingly, while the stellar parameters (e.g. temperature, surface abundances) suggest broadly similar evolutionary stages for these objects, we find that the nebular properties are rather diverse. Nebular masses inferred from M_{dust} are found to span more than an order of magnitude in range, with no apparent correlation with the luminosity of the central source. Likewise, the analysis of the present data for the MSX sources suggest that both nebular formation histories (single versus multiple "ejection" events) and chemistries (O-rich or mixed O+C-rich) may differ for nebulae around stars with similar physical properties, although we caution that further observations with both higher spatial and wavelength resolution are required to confirm these results.

Similar results are found upon consideration of the properties of the nebulae around known and candidate LBVs. Given the similarity in stellar parameters and the *range* of nebular parameters of the MSX sources and (c)LBVs it is tempting to identify the MSX ring sources as cLBVs. While the baseline of observations for many sources is poor, AFGL 2298 and the Pistol Star – both of which may be considered members of the group of MSX sources – already demonstrate significant spectroscopic and photometric variability. Spectroscopic variability has been reported for G79.49+0.26, while the results presented here indicate that G24.73+0.69 is also photometrically, and probably spectroscopically, variable. Finally, comparison of our photometric data for G26.47+0.02 to archival 2 mass fluxes suggest that it too may be photometrically variable, while only one epoch of observations exist for Wra 17-96. Therefore, we propose the MSX ring nebulae sources to be new cLBVs, and suggest that further monitoring will reveal variability in most, if not all, objects, confirming them as bona fide LBVs.

Acknowledgements. This article is partially based on observations obtained in service time with the United Kingdom Infrared Telescope, which is operated by the Joint Astronomy Centre on behalf of the U.K. Particle Physics and Astronomy Research Council. We wish to thank the observers for the efforts in obtaining these data. This publication makes use of data products from the Two Micron All Sky Survey, which is a joint project of the University of Massachusetts and the Infrared Processing and Analysis Center/California Institute of Technology, funded by the National Aeronautics and Space Administration and the National Science Foundation. VL acknoledges support from Russian Federal Program "Integration", grant B0029 and VL and AA thank Italian colleagues for their hospitality and help during observations at Campo Imperatore.

References

Becker, R. H., White, R. L., Helfand, D. J., & Zoonematkermani, S. 1994, ApJS, 91, 347
Bohannan, B., & Crowther, P. A. 1999, ApJ, 511, 374
Bohigas, J., Tapia, M., Ruiz, M. T., & Roth, M. 2000, MNRAS, 312, 295
Clark, J. S., Steele, I. A., & Langer, N. 2000, ApJ, 541, L67
Clark, J. S., Larionov, V. M., Crowther, P. A., Egan, M. P., & Arkharov, A. 2003, A&A, 403, 653
Condon, J. J., Cotton, W. D., Greisen, E. W., et al. 1998, AJ, 115, 1693
Crowther, P. A. 1997, in Luminous Blue Variables: Massive Stars in Transition, ed. A. Nota, & H. Lamers, ASP Conf. Ser., 120, 51
Drissen, L., Crowther, P. A., Smith, L. J., et al. 2001, ApJ, 546, 484
Egan, M. P., Leung, C. M., & Spagna, G. F. 1988, Comput. Phys. Commun., 48, 271
Egan, M. P., Clark, J. S., Mizuno, D. R., et al. 2002, ApJ, 572, 288
Figer, D. F., Najarro, F., Morris, M., et al. 1998, ApJ, 506, 384
Figer, D. F., Morris, M., Geballe, T. R., et al. 1999, ApJ, 525, 759
Geballe, T. R., Najarro, F., & Figer, D. F. 2000, ApJ, 530, L97
Glass, I. S., Matsumoto, S., Carter, B. S., & Sekiguchi, K. 1998, MNRAS, 304, L10
Higgs, L. A., Wenker, H. J., & Landecker, T. L. 1994, A&A, 291, 295
Hillier, D. J., & Miller, D. L. 1998, ApJ, 496, 407
Hillier, D. J., Crowther, P. A., Najarro, F., & Fullerton, A. W. 1998, A&A, 340, 483
Hillier, D. J., Davidson, K., Ishibashi, K., & Gull, T. 2001, ApJ, 553, 837
Humphreys, R. M., & Davidson, K. 1994, PASP, 106, 1025
Hutsemekers, D. 1997, in Luminous Blue Variables: Massive Stars in Transition, ed. A. Nota, & H. Lamers, ASP Conf. Ser., 120, 316
Jager, C., Molster, F. J., Dorschner, J., et al. 1998, A&A, 340, 483
Krauss, M., Hanson, M., & Voors, R. H. M. 2000, A&AS, 197, 4412
Lamers, H. J. G. L. M., Nota, A., Panagia, N., Smith, L. J., & Langer, N. 2001, ApJ, 551, 764
Meaburn, J., Lopez, J. A., & O'Connor, J. 1999, ApJ, 516, L29
Meaburn, J., O'Connor, J. A., Lopez, J. A., et al. 2000, MNRAS, 318, 561
Mill, J. M., O'Neil, R., Price, S. D., Romick, G. Uy. M., & Gaposchkin, E. M. 1994, J. Spacecraft Rockets, 31, 900
Moneti, A., Blommaert, J., Najarro, F., Figer, D. F., & Stolovy, S. 1999, in The Universe as seen by ISO (ESA-SP 427), ed. P. Cox, & M. F. Kessler, 723
Morris, P. W., Eenens, P. R. J., Hanson, M. M., Conti, P. S., & Blum, R. D. 1996, ApJ, 470, 597
Morris, P. W., Naters, L. B. F. M., Barlow, M. J., et al. 1999, Nature, 402, 502
Nota, A., Livio, M., Clampin, M., & Sculte-Ladbeck, R. 1995, ApJ, 448, 788
Nota, A., Pasquali, A., Marston, A. P., et al. 2002, AJ, 124, 2920
Pasquali, A. 1997, in Luminous Blue Variables: Massive Stars in Transition, ed. A. Nota, & H. J. G. L. M. Lamers (San Francisco: ASP), ASP Conf. Proc., 120, 13

Pasquali, A., Nota, A., Smith, L. J., et al. 2002, AJ, 124, 1625
Pollack, J. B., Hollenbach, D., Beckwith, S., et al. 1994, ApJ, 421, 615
Price, S. D., Egan, M. P., Carey, S. J., Mizuno, D. R., & Kuchar, T. A. 2001, AJ, 121, 2819
Robberto, M., & Herbst, T. M. 1998, ApJ, 498, 400
Smith, L. J., Crowther, P. A., & Prinja, R. K. 1994, A&A, 281, 833
Smith, L. J., Nota, A., Pasquali, A., et al. 1998, ApJ, 503, 278
Stephenson, C. B. 1992, AJ, 103, 263
Subrahmanyan, R., Ekers, R. D., Wilson, W. E., Goss, W. M., & Allen, D. A. 1994, MNRAS, 268, 304
Ueta, T., Meixner, M., Dayal, A., et al. 2001, APJ, 548, 1020
van Genderen, A. M. 2001, A&A, 366, 508
van Kerkwijk, M. H., Kulkarni, S. R., Matthews, K., & Neugebauer, G. 1995, ApJ, 444, L33
Voors, R. H. M., Waters, L. B. F. M., Trams, N. R., & Kaufl, H. 1997, A&A, 321, L21
Voors, R. H. M., Waters, L. B. F. M., Morris, P. W., et al. 1999, A&A, 341, L67
Voors, R. H. M., Waters, L. B. F. M., de Koter, A., et al. 2000a, A&A, 356, 501
Voors, R. H. M., Geballe, T. R., Waters, L. B. F. M., Najarro, F., & Lamers, H. J. G. L. M. 2000b, A&A, 362, 236
Waters, L. B. F. M., Izumiura, H., Zaal, P. A., et al. 1996, A&A, 313, 866
White, S. M. 2000, ApJ, 539, 851
Whittet, D. C. B. 1992, Dust in the Galactic Environment (Bristol: Inst. Phys.)